

Using Complementary NMR Data Sets to Detect Inconsistencies and Model Flaws in the Structure Determination of Human Interleukin-4

Lorna J. Smith,[†] Wilfred F. van Gunsteren,[‡] and Niels Hansen^{*,¶}

Department of Chemistry, Inorganic Chemistry Laboratory, South Parks Road, Oxford, OX1 3QR, UK, Laboratory of Physical Chemistry, CH-8093 Zürich, Switzerland, and Institute of Thermodynamics and Thermal Process Engineering, D-70569 Stuttgart, Germany

E-mail: hansen@itt.uni-stuttgart.de

Phone: +49 (0)711 685 66112. Fax: +49 (0)711 685 66140

*To whom correspondence should be addressed

[†]University of Oxford

[‡]Swiss Federal Institute of Technology, ETH

[¶]University of Stuttgart

Abstract

The derivation of protein structure from values of observable quantities measured in NMR experiments is a rather non-trivial task due to (i) the limited number of data compared to degrees of freedom of a protein, (ii) the uncertainty inherent to the function connecting an observable quantity to molecular structure, (iii) the finite quality of biomolecular models and force fields used in structure refinement, and (iv) the conformational freedom of a protein in aqueous solution, which requires extensive conformational sampling and appropriate conformational averaging when calculating or restraining to sets of NMR data.

The protein interleukin-4 (IL-4) has been taken as a test case using NOE distances, S^2 order-parameters and 3J -couplings as test data and the former two types of data as restraints. It is shown that by combining sets of different, complementary NMR data as restraints in MD simulation inconsistencies in the data or flaws in the model and procedures used to derive protein structure from NMR data can be detected. This leads to an improved structural interpretation of such data particularly in more mobile loop regions.

Introduction

The first 3-dimensional model structures of proteins were obtained by interpretation of X-ray diffraction intensities using a model for the covalent structure in combination with electron density maps obtained by Fourier transform of the crystallographic structure factors.^{1,2} Much later the introduction of multi-dimensional NMR techniques³ allowed for the derivation of 3-dimensional model structures of a protein based on the interpretation of NMR spectroscopic signals.⁴ Today, the protein data bank (PDB)⁵ holds thousands of 3-dimensional model structures, mostly built on the basis of X-ray crystallographic data, but also on a variety of NMR solution data.

Nuclear Overhauser Effect (NOE) intensities can be used to derive bounds on particular

atom-atom distances. Residual Dipolar Couplings (RDC) can be used to infer angles of bond vectors with the direction of the magnetic field.⁶ Both types of observable quantities have been used to derive protein model structures. Chemical shielding values for particular atoms are relatively easy to measure, but due to the uncertainty of their relation to local molecular structure they cannot straightforwardly be used to derive protein structure. However, progress has been made in strategies that combine chemical shift data with fragment-based approaches.⁷ 3J -couplings can also be relatively easily measured, if their values are not small, but their conversion to structural information based on the Karplus relation⁸ introduces a rather large uncertainty, which severely limits their value for protein structure determination. Finally, NMR relaxation measurements can be used to derive values for so-called S^2 order parameters for particular bond vectors, which represent the degree of variability of the bond vector which respect to the molecular frame.⁹

The use of NMR S^2 order parameters in structure determination is less straightforward than for the other quantities mentioned, because the order parameter S^2 is not a function of a single molecular configuration, but of the long-time tail of the time-correlation function of a vector along a particular bond or line connecting two atoms of a molecule. This long-time limit or tail can be expressed¹⁰ as a time-average of a function f of the molecular configuration \vec{r} , $S^2(\langle f(\vec{r}) \rangle)$. Using an exponential damping function $\exp(-t/\tau_{S^2})$ in the time-averaging the simulated trajectory can be biased such that a set of target S^2 values derived from experiment is reproduced in the simulation.¹¹ For low target S^2 values, the use of S^2 order-parameter restraining enhances the orientational mobility of the corresponding bond vector and thus the local sampling. Application of S^2 order-parameter restraints enabled the convergence of local structure in a flexible lip region of λ -lysozyme in S^2 -restrained MD simulations starting from two different X-ray crystal structures.¹² When applied to the human growth hormone, it allowed the identification of transitions between α - and 3_{10} -helical structure in the center of helices.¹³

Although the spatial structure of a protein in solution is of more relevance to its func-

tioning in a cell than that of a protein in a crystal, the latter structures are more widely used, e.g. in protein engineering and drug design. This is among others due to the difference in accuracy between model structures derived from X-ray diffraction data for crystals and derived from NMR spectroscopic data for proteins in solution.

1. Since the number of independent diffraction intensities is generally large, of the same order of magnitude as the number of protein degrees of freedom, only a relatively simple molecular model and interaction function, e.g. only containing values for bond lengths, bond angles and atom sizes, is needed to derive a spatial structure. NMR data are less abundant and contain short-range distance information (NOE) or information on the directionality of particular bonds (RDC). This implies that the quality of the molecular model and force field used to convert NMR data to structure is of greater importance and thus has its effect on the reliability of the protein structure derived.
2. Generally, relatively simple molecular models, lacking long-range Coulombic interaction terms, are used in modelling based on NMR data.¹⁴
3. Since the structure determination problem is an under-determined one, searching and sampling the conformational space of a protein in solution is of much greater importance than for the crystal with its limited protein mobility. Searching and sampling conformational space using MD simulation was thus first introduced in structure refinement based on NMR data^{15,16} and later in structure refinement based on X-ray diffraction data.^{17,18}
4. Not only measured data possess a degree of uncertainty, but the procedures to convert values of observable quantities into spatial structures do inevitably introduce more uncertainty. This effect is for the mentioned NMR quantities (NOEs, RDCs, etc.) much larger than for the conversion of X-ray diffraction intensities to electron density.
5. Measured values of observable quantities are generally averages over time and space or molecules. The conformational distribution over which their averaging is performed will be wider in solution than in a crystal. This makes accounting for multiple conformations of a protein when deriving a structural model based on NMR data more important than

when deriving crystal model structures.

These issues make deriving a structural model for a protein on the basis of NMR data a rather non-trivial task, beset with a variety of pitfalls and ambiguities.¹⁹ One way to reduce the latter is by combining NMR data of different types, e.g. NOEs, S^2 order parameters and 3J -couplings in structure determination or refinement of a particular protein. If these different types of data are independent and complementary, combining them may yield hints at inconsistencies or flaws in the particular type of NMR data or their conversion to structure. In addition, combining complementary data, such as NOEs yielding structural information (atom-atom distance bounds) and S^2 order parameters representing degree of flexibility of bond vectors, may lead to a more reliable representation of the conformational ensemble of the protein. These two issues are investigated for the 129-residue protein interleukin-4 (IL-4), for which NOE, backbone N-H S^2 order parameter, and backbone $^3J_{\text{HNH}\alpha}$ -coupling data are available, obtained from NMR experiments at similar thermodynamic conditions.^{20,21}

Interleukin-4 (IL-4) is a pleiotropic type 1 cytokine, which plays a central role in the control and regulation of the immune and inflammatory systems.²² The most notable functions of IL-4 include the development of T-helper cells to a type 2 cytokine-producing phenotype. IL-4 evokes a cellular response by promoting the formation of a heterodimeric receptor complex in the plasma membrane.²³⁻²⁵ The spatial structure of IL-4 under native conditions has been established in solution^{20,26} and in crystals.²⁷⁻²⁹ IL-4 is one of the four helix bundle cytokines³⁰ that are characterised by antiparallel juxtaposed helices A, B, C, D and two long end-to-end loops, loops AB and CD, which are connected by a short β -sheet packed against helices B and D (Figure 1). The overall structure is highly compact and globular with a predominantly hydrophobic core. Smith et al.³¹ have thoroughly compared the four independently determined structures of human recombinant IL-4 and they found the core of the four helix bundle to be very similar in all the structures, except for differences in the loop regions that are known to be mobile in solution.²¹

The following sets of experimental data were used in the analysis of the unrestrained and

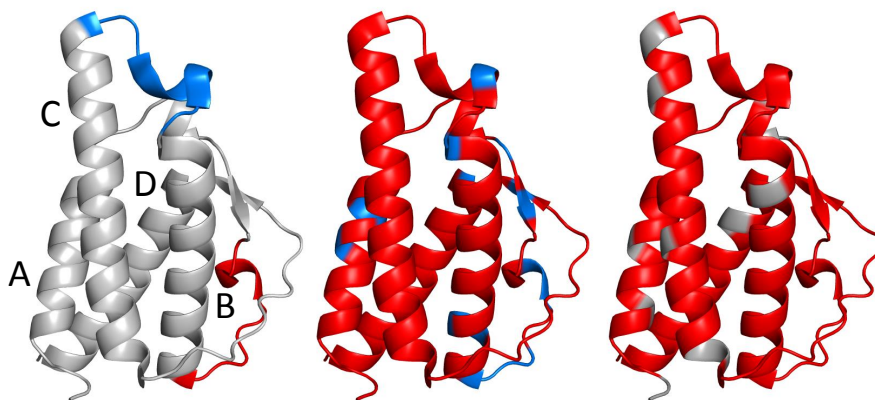


Figure 1: Ribbon representations of the structure of IL-4 as derived from X-ray diffraction data.³² Left panel: the four helices A, B, C and D are indicated, the AB2 loop (residues in 31-40) in red, the BC loop (residues 60-71) in blue. Middle panel: the residues with atoms for which NOE distance bounds derived from NMR data are available²⁰ in red, and those for which one or more of the NOEs were found to be questionable in blue (NOE bounds 14 NH – 15 HB1, 15 HD21 – 14 HA, 34 HA – 35 HN, 39 HN – 40 HN, 44 HN – 45 HB1, 27 HA – 29 HN, 35 HA – 38 HN, 107 HA – 109 HN, 12 HA – 15 HB1, 60 HA – 63 HG2, 25 HA – 109 HA). Right panel: the residues for which backbone N-H S^2 order parameters derived from NMR data are available²¹ in red.

restrained MD simulations.

1. NOE: a set of 1657 atom-atom distance bounds.²⁰
2. NOEred: a set of 1646 distance bounds, set NOE minus 11 bounds.
3. $^3J_{\text{HN}\alpha}$: a set of 66 $^3J_{\text{HN}\alpha}$ -couplings.²⁰
4. S^2 : a set of 113 backbone N-H S^2 order parameters.²¹

Unrestrained (NR) and restrained MD simulations were performed, the latter with the following sets of restraints as target values.

1. NOE
2. NOEred
3. S^2
4. NOE and S^2
5. NOEred and S^2

The set of NOE distance bounds had been obtained²⁰ from NOE peak intensities classified as very strong, strong, medium or weak. By studying the intensities of cross-peaks in secondary structure elements where interproton distances are known, upper distance bounds of 0.25, 0.3, 0.4, and 0.5 nm were chosen for the mentioned NOE intensities, respectively.^{20,33}

The set ${}^3J_{\text{HN}\alpha}$ was not used as restraints because (i) many ${}^3J_{\text{HN}\alpha}$ -couplings (those in helices) have small values, which are difficult to determine precisely, (ii) the remaining ${}^3J_{\text{HN}\alpha}$ -couplings have values in the range 5-8 Hz and belong to residues in the long loops, for which conformational averaging over periods much longer than tens of nanoseconds may be needed, and (iii) the Karplus relation that connects the φ torsional angle to a ${}^3J_{\text{HN}\alpha}$ -coupling possesses a rather large uncertainty of 1-2 Hz.³⁴

The restraining functions for atom-atom distance bounds³⁵ and S^2 order parameters¹¹ depend on two parameters, the weight or force constant K determining the strength of the restraining term in relation to the other potential energy terms of the force field used, and the memory relaxation time τ determining the period over which averaging is performed. These four parameters were varied in order to determine their influence on the resulting conformational ensembles. In total more than 40 different 20 ns MD simulations were performed and analysed. Only the most significant results are reported here, i.e. NOE distance-bound restraining with $K_{\text{NOE}} = 6000 \text{ kJ mol}^{-1} \text{ nm}^{-2}$ and $\tau_{\text{NOE}} = 20 \text{ ps}$ or 1000 ps , and S^2 order-parameter restraining with $K_{S^2} = 300 \text{ kJ mol}^{-1}$ and $\tau_{S^2} = 20 \text{ ps}$ or 200 ps .

Methods

Earlier MD simulations of IL-4 have been performed³⁶ using the GROMOS force fields 45A3 of 2000³⁷ and 53A6 of 2004.³⁸ The simulations presented here use the GROMOS11 software package^{39,40} and an improved force-field parameter set 54A7 of 2011.⁴¹ Initial coordinates were taken from the X-ray structure of IL-4 (Protein Data Bank entry: 2B8U).³² To model pH 6 conditions, the Asp and Glu side chains and the C-terminus were not protonated. His

was doubly protonated, except for His 76 which was only protonated at N_ϵ . The simple-point-charge (SPC) water model⁴² was used to describe the 12549 solvent molecules present in the rectangular periodic box. 11 Cl^- counterions were present to neutralize the +11 e charge of the protein. All bonds and the bond angle of the water molecules were kept rigid with a geometric precision of 10^{-4} using the SHAKE algorithm,⁴³ allowing for a 2 fs MD time step in the leap-frog algorithm⁴⁴ used to integrate the equations of motion. For the non-bonded interactions a triple-range method⁴⁵ with cut-off radii of 0.8/1.4 nm was used. Short-range van der Waals and electrostatic interactions were evaluated every time step based on a charge-group pairlist.³⁹ Medium-range van der Waals and electrostatic interactions, between pairs at a distance larger than 0.8 nm and shorter than 1.4 nm, were evaluated every fifth time step, at which time point the pairlist was updated, and kept constant between updates. Outside the larger cut-off radius a reaction-field approximation^{46,47} was used with a relative dielectric permittivity of 61.⁴⁸

An equilibration scheme consisting of five short 20 ps simulations at temperatures of 60 K, 120 K, 180 K, 240 K and 307 K was used at constant volume. During the first four of the equilibration periods the solute atoms were harmonically restrained to their positions in the initial structures with force constants of 25000, 2500, 250 and 25 $\text{kJ mol}^{-1}\text{nm}^{-2}$. Following this equilibration, simulations were performed at a temperature of 300 K and a pressure of 1 atm using the weak-coupling algorithm, with relaxation times of $\tau_T = 0.1$ ps and $\tau_p = 0.5$ ps and an isothermal compressibility of $4.575 \times 10^{-4} (\text{kJ mol}^{-1}\text{nm}^{-3})^{-1}$. Solute and solvent were separately coupled to the heat bath. The centre of mass motion of the system was removed every 1000 time steps.

The GROMOS force fields treat aliphatic carbons as united CH, CH_2 and CH_3 atoms. Thus calculated interproton distances involving the aliphatic hydrogen atoms were calculated using virtual (for CH, and prochiral CH_2)⁴⁹ and pseudo (for CH_3)⁵⁰ atomic positions for these hydrogen atoms.³⁹ The pseudo-atom NOE bound distance corrections of Wüthrich et al.⁵⁰ were used, see e.g. ref. 19.

The sets of NOE distance bounds, S^2 order-parameter target values, and observed $^3J_{\text{H}_\text{N}\text{H}_\alpha}$ -couplings to compare with are specified in Tables S1-3 of Supporting Information, together with the values of the simulation without any restraining (NR) and of the simulation NOEred_20_ S^2 _200 with NOE distance and S^2 order-parameter restraining.

In view of the uncertainty inherent to the calculation of NOE bounds and r^{-3} averaged distances, S^2 order parameters and $^3J_{\text{H}_\text{N}\text{H}_\alpha}$ -couplings, we consider deviations between MD simulated values and values derived from experiment of less than 0.1 nm (NOE), 0.2 (S^2) and 2 Hz (3J -couplings) as insignificant. In addition, experimentally derived order parameters that were greater than 0.9 were set to a target value of 0.9.

Results and Discussion

S^2 Order-parameter restraining

The simulation without any restraining (NR) shows 25 NOE distance bound violations larger than 0.1 nm of which only one (32 HA – 103 HG#, no. 1543 in Table S1) is larger than 0.3 nm (Table 1, NR). It shows 8 S^2 order parameter deviations larger than 0.2 of which two (residues 62 and 127) are larger than 0.3 (Table 2, NR, and Table S2). It shows 6 $^3J_{\text{H}_\text{N}\text{H}_\alpha}$ -couplings deviating more than 2 Hz of which one (residue 96) deviates more than 3 Hz (Table 3, NR, and Table S3). When applying S^2 order-parameter restraints, either with $\tau_{S^2} = 20$ ps (S^2 _20) or with $\tau_{S^2} = 200$ ps (S^2 _200), the deviation from the measured S^2 values decreases, in particular using the longer averaging time (Table 2, S^2 _20 and S^2 _200) of 200 ps. The deviations from the measured $^3J_{\text{H}_\text{N}\text{H}_\alpha}$ -couplings do not change much (Table 3) although all the simulations show fewer deviations than the starting crystal structure. However, the number of NOE distance bound violations beyond 0.1 nm is reduced from 25 to 16 (Table 1) with no significant difference between S^2 _20 and S^2 _200. Thus S^2 restraining improves the agreement with experiment for the NOEs and has little effect on the agreement between simulation and experiment for the $^3J_{\text{H}_\text{N}\text{H}_\alpha}$ -couplings.

NOE distance restraining: inconsistencies?

Next restraining to the set of 1657 NOE distance bounds was performed. As expected, only small NOE bound violations (< 0.05 nm) were observed (Table 1, NOE_20 and NOE_1000), six more for the larger averaging time $\tau_{\text{NOE}} = 1000$ ps than for $\tau_{\text{NOE}} = 20$ ps. The measured $^3J_{\text{H}_\text{N}\text{H}_\alpha}$ -couplings were not much better reproduced than in the unrestrained or S^2 -restrained simulations, but the deviations from the experimentally derived S^2 values increased strongly, to 7 deviations larger than 0.3 for NOE_20 and even 19 larger than 0.3 for NOE_1000 (Table 2). Even when NOE and S^2 restraints are applied together there are still a significant number of larger deviations from S^2 values derived from experiment. The agreement for the S^2 values was not improved by increasing the force constant K_{S^2} for S^2 restraining. Apparently the set of NOEs was not compatible with the set of S^2 order parameters. This led us to reanalyse the original NMR spectra from which two NOEs (35HA-38HN and 60HA-63HG2, nos. 602 and 831 in Table S1) may have been incorrectly assigned, in one case due to peak overlap and in the other case due to chemical shift degeneracy. A more detailed analysis of the NOE data set using the X-ray crystal structure of IL-4 used as the starting structure for the simulations was then performed. In addition, instantaneous restraining ($\tau_{\text{NOE}} = 0$ ps) was applied for the NOE set (NOE_IR) in order to detect atom-atom distance restraints with a high restraining energy hinting at incompatibility with the minimum energy conformations as allowed by the force field. On the basis of this analysis a further nine NOEs were removed yielding the NOEred set of 1646 NOE distance bounds (see Table S1). Interestingly, only one (25 HA - 109 HA, no. 1429 in Table S1) of these 9 NOEs is longer range. The others are sequential or short range (i, i+2 or i+3) NOEs with strong or medium intensities. The intensities of these NOEs may have been increased by spin diffusion effects with the 100 ms NOE mixing time used.²⁰ Consequently, the upper distance bounds used for these NOE restraints may be too short.

The questionable NOE distance bounds could have been further investigated using a relaxation-matrix calculation analysis⁵¹⁻⁵⁴ in which several aspects of intra-molecular flexi-

bility that influence NOE cross-relaxation rates are accounted for.⁵² Three major effects of neglecting intra-molecular dynamics can be distinguished.

1. Intra-protein dynamics lead to fluctuations in the interproton distances.
2. The overall correlation times of the motions of interproton vectors contain contributions from both tumbling motions and internal dynamics and are thus different for each proton pair.
3. Due to the superposition of overall rotations and possibly various types of internal motions, the overall time correlation function is not a single exponential and thus the spectral density is not a simple Lorentz function.

A relaxation matrix analysis of a polypeptide showed⁵² that the long-distance NOEs are probably mainly sensitive to the distance average and that the effects of different correlation times and the shape of the spectral density functions have a minor impact, whereas they play a more important role for pairs which are separated only by a few bonds.

NOE distance restraining with a reduced set of bounds

Using the NOEred set of 1646 NOE bounds as restraints the number of NOE bound violations is not significantly changed keeping in mind that the NOEred_20 and NOEred_1000 simulations have 11 less restraints than the NOE_20 and NOE_1000 ones (Table 1). However, the agreement with the experimental S^2 values is significantly improved when restraining to the NOEred set. The deviations from the measured $^3J_{\text{H}_\text{N}\text{H}_\alpha}$ -couplings have also become slightly less. In addition, the distance restraining energy is halved and the protein potential energy is lowered (Table 4).

Combined NOE distance and S^2 order-parameter restraining

Using the reduced NOE data set NOEred for distance restraining in combination with the S^2 order-parameter set, the agreement with the experimental data is much improved, in

particular when using $\tau_{\text{NOE}} = 20$ ps and $\tau_{S^2} = 200$ ps (NOEred_20_200). There are no NOE bound violations beyond 0.05 nm, only two S^2 order parameters that deviate more than 0.1 from the values inferred from experiment, and the number of $^3J_{\text{H}_\text{N}\text{H}_\alpha}$ -couplings deviating more than 0.5 Hz from the measured values is the lowest for simulation NOEred_20_200.

Variation of the averaging times τ_{NOE} and τ_{S^2}

Extending the memory relaxation time τ_{NOE} from 20 ps to 1 ns increases the number of NOE bound violations in all simulations, except the ones with in addition S^2 order-parameter restraining with $\tau_{S^2} = 200$ ps (Table 1). It also strongly increases the deviations from the S^2 values derived from experiment (Table 2), and the agreement with measured $^3J_{\text{H}_\text{N}\text{H}_\alpha}$ -couplings is not improved (Table 3). Using $\tau_{\text{NOE}} = 20$ ps seems more appropriate than $\tau_{\text{NOE}} = 1$ ns. The latter value is of the same order of magnitude as the rotational tumbling time of 7.6 ns of IL-4.²¹ Indeed, the r^{-3} -averaging time τ_{NOE} for the NOE distances should be chosen much shorter than the tumbling time of the protein.

Extending the memory relaxation time τ_{S^2} from 20 ps to 200 ps yields much better agreement with the S^2 values derived from experiment in all simulations, while no significant changes in agreement with experiment for NOE bounds and $^3J_{\text{H}_\text{N}\text{H}_\alpha}$ -couplings are observed. In contrast to an NOE atom-atom distance, a S^2 order parameter is defined as a long-time average, which however can be converted to an ensemble average.¹⁰ Thus the averaging time should be chosen as long as possible, but much shorter than the length of the simulation in order to secure sufficient statistics over independent data points. This condition is still fulfilled for $\tau_{S^2} = 200$ ps used in 20 ns simulations.

Signalling inconsistencies in data or refinement procedures

The inconsistency of the different data sets was detected through the calculation of different quantities.

1. Figure 2 shows the backbone H-N S^2 order parameters derived from experiment and

simulations NR, NOE_20, NOEred_20, NOE_20_ S^2 _20 and NOEred_20_ S^2 _200. The agreement with experiment worsened by the NOE distance restraining using the full set of 1657 NOE bounds, and it improved upon removal of the 11 questionable bounds.

2. The distance restraining energies per distance restraint were quite large for the full NOE bound set (Table 4), and so were intra-protein energies, which could be lowered by removal of the 11 questionable NOE bounds.

3. Figure 3 shows the backbone N-atom root-mean-square fluctuation for 9 simulations. Using the full NOE bound set produced large fluctuations, in particular for $\tau_{\text{NOE}} = 1$ ns. The NOEred_20_ S^2 _200 simulation showed backbone atom-positional fluctuations closest to the ones of the unrestrained simulation.

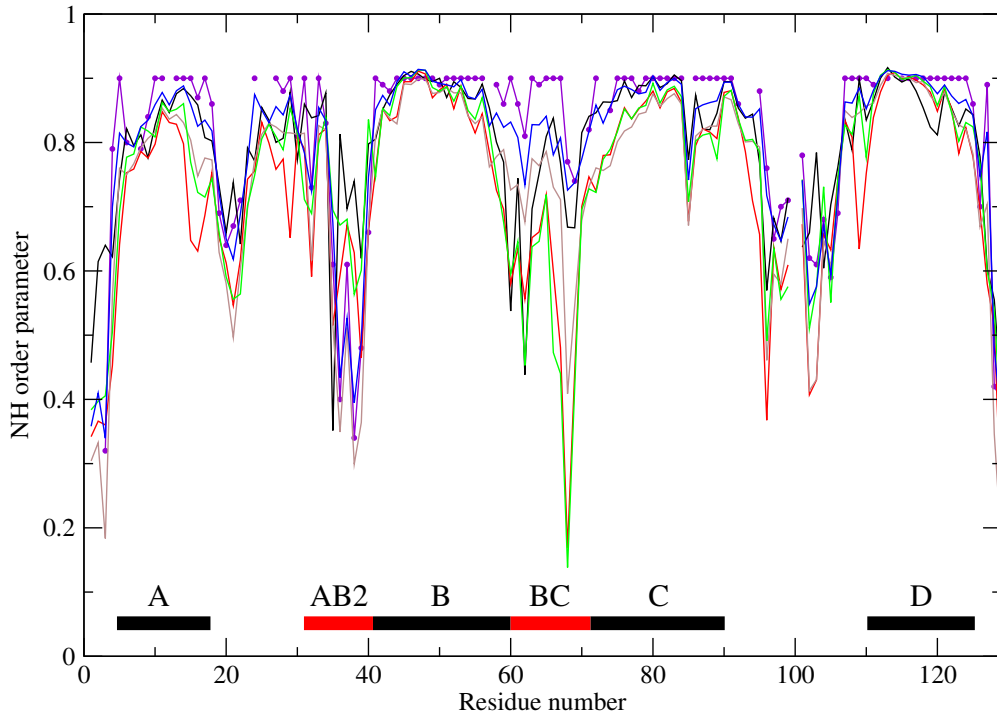


Figure 2: Backbone N-H bond vector S^2 order parameters as function of residue number of IL-4. Purple dots and lines: values derived from NMR relaxation data.²¹ Values from simulation NR in black, from NOE_20 in red, from NOE_20_ S^2 _20 in brown, from NOEred_20 in green, and from NOEred_20_ S^2 _200 in blue. Only adjacent residues for which S^2 values are available are connected by the lines. Solid bars indicate the position of the helices A to D (in black) and the AB2 and BC loops (in red).

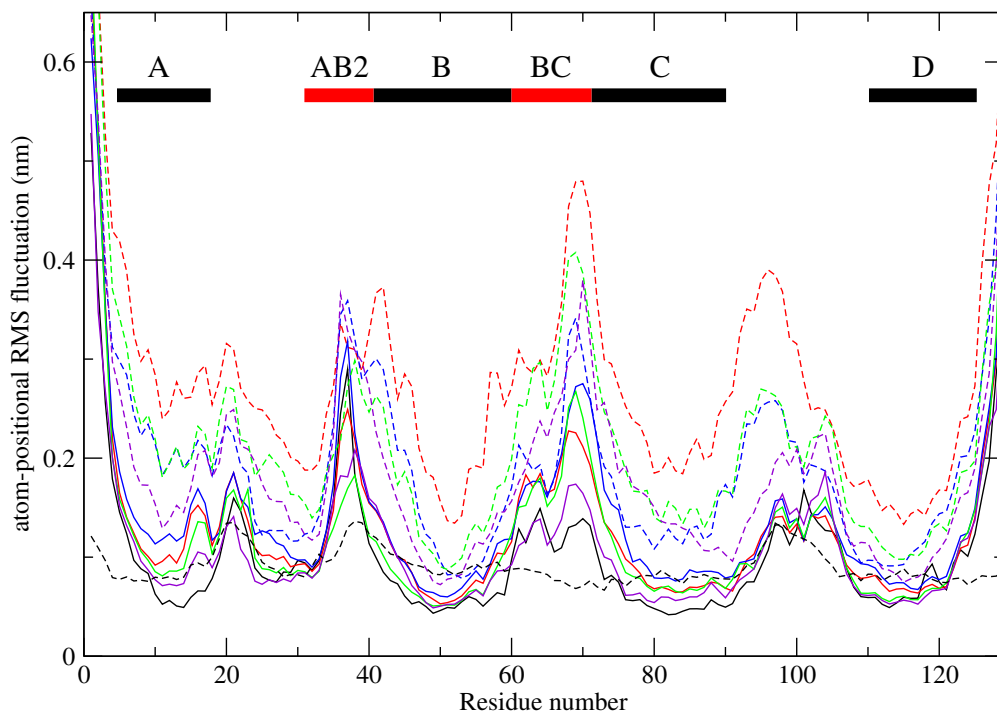


Figure 3: Backbone N-atom positional root-mean-square fluctuation (RMSF) in nm from the different 20 ns MD simulations. Black: unrestrained (NR); red: NOE_20 (solid) and NOE_1000 (dashed); blue: NOE_20_ S^2 _20 (solid) and NOE_1000_ S^2 _20 (dashed); green: NOEred_20 (solid) and NOEred_1000 (dashed); purple: NOEred_20_ S^2 _200 (solid) and NOEred_1000_ S^2 _200 (dashed). Solid bars indicate the positions of the helices A to D (in black) and the AB2 and BC loops (in red). The X-ray crystallographic B-factors³² are represented as RMSF values $(3B_i/(8\pi^2))^{\frac{1}{2}}$ (black, dashed).

Structural effects in the AB loop and CD loop

The AB loop and CD loop are long and run the length of the IL-4 molecule (Figure 1). These loop regions of the molecule show larger B-factors as obtained from X-ray crystallographic structure refinement (Figure 3) and relatively lower backbone N-H bond vector S^2 order parameters in solution (Figure 2). There is a short region of β -sheet connecting the middle of the AB loop to the end of the CD loop (residues 28-30 and 106-108). This splits the AB loop into two sections, AB1 (residues 18-27) and AB2 (residues 31-40). Comparison of two different X-ray crystal structures have shown differences in the AB2 loop around residues 37 and 38, where the electron density is particularly diffuse.³¹

In the 2B8U X-ray structure, used as starting structure for the simulations, residues 32 to

34 in the AB2 loop region form helical turns. These are lost in the initial energy minimisation of IL-4 and in the unrestrained (NR) simulation an additional β -bridge hydrogen bond is formed between residues 36 and 103 (Table 5). It is, however, lost in all restraining MD simulations except NOEred_20_ S^2 _200.

In the AB2-loop region, S^2 order-parameter restraining induces some helical structure fluctuating between α - and 3_{10} -helical types for residues 31-36. Using the full set of 1657 NOEs as distance bounds in restraining, mixed α - and 3_{10} -helical structure is observed additionally for residues 34-39. Combined with S^2 order-parameter restraining the helicity extends along the whole AB2 loop region. It is reduced, however, when the reduced set of 1646 NOE bounds is used in the restraining. This shows that for this rather flexible region of IL-4 the conformational ensemble derived on the basis of force-field and NMR data is sensitive to details of the latter and to the way structures are derived from measured data.

The BC loop (residues 60-71) does not show low S^2 order parameters experimentally, but ^{15}N relaxation studies indicate that residues 63 and 67 have large T_1/T_2 ratios suggesting motion on a millisecond time scale.²¹ In the absence of NOE distance restraining this loop adopts α -helical structure, which is also present in the X-ray crystal structure (residues 63-66). When NOE distance restraints are applied a mixture of α - and 3_{10} -helical hydrogen bonds is present (Table 5), but less for the reduced set of NOE bounds. Again the structural preferences depend on the force field, type of NMR data and the way these are imposed in the simulations.

Conclusion

The combination of different types of NMR data available for the protein IL-4 in aqueous solution when deriving structural information was investigated using different sets of measured data and values of the parameters used in the restraining functions that were added to the GROMOS 54A7 interaction function used to model the protein. The memory relax-

ation time τ_{NOE} that governs the averaging of the distance between atoms for which NOE distance bounds derived from experiment are available, should be chosen much smaller than the rotational tumbling time of the protein, which is generally of the order of nanoseconds. In contrast, the memory relaxation time τ_{S^2} that governs the averaging inherent to the definition of the S^2 order parameter as a long-time tail of the N-H bond vector autocorrelation function, should be chosen as long as possible, but much shorter than the MD simulation length in order to secure sufficient statistics. S^2 order-parameter restraining as proposed in ref. 11 enhances the conformational sampling, as does NOE atom-atom distance restraining as long as time-averaging is accounted for.¹⁶ The agreement of the various (un)restrained MD simulations with the set of 66 $^3J_{\text{H}_\text{N}\text{H}_\alpha}$ -couplings derived from NMR experiments did neither show sensitivity to changes in restraining parameters nor to the application of different sets of restraints. This is probably due to the large uncertainty in the calculated 3J -couplings, due to the empirical nature of the Karplus relation connecting torsional angle with 3J -coupling and to the long time scale of motions that contribute to 3J -couplings, which may be much longer than that of MD simulations. However, it is interesting that all the MD simulations showed fewer large $^3J_{\text{H}_\text{N}\text{H}_\alpha}$ -coupling deviations than the starting crystal structure.

The possible occurrence of inconsistencies between values of quantities derived from measured data or flaws in the model and procedures to derive structural information from NMR data was investigated in different ways.

1. Identification of NOE bounds violated in an X-ray crystal structure may help to detect inappropriate NOE bounds. A relaxation-matrix calculation of NOE intensities may also help.
2. A rather high distance restraining energy in restrained MD simulation may hint at an inappropriate NOE bound, in particular when instantaneous restraining (IR) is applied.
3. Too large atom-positional RMS fluctuations are an indication of inconsistencies in the data set used for restraining.
4. When different types of data sets (NOEs, S^2 order parameters, 3J -couplings) are avail-

able, restraining to one data set should not significantly destroy the agreement between simulation and experimental data for another data set.

In the case of IL-4 such investigations led to the reconsideration of the derivation of a number of NOE bounds, some of which turned out to be questionable. MD simulations with a reduced set of 1646 NOE distance bounds and a set of backbone N-H bond vector S^2 order-parameter restraints could then be used for a structural interpretation of the NMR data. The flexible parts of IL-4, the AB and CD loops do not adopt a particular conformation but show alternating helical structures, which may allow adaptation upon ligand binding.

This case study illustrates the uncertainty inherent to model structures derived from NMR data and ways to reduce it by using sets of different complementary types of data.

Table 1: Number of NOE atom-atom distance bound violations in the various MD simulations^{a)}.

Simulation	Size of NOE distance bound violation (in nm)				
	0.0-0.05	0.05-0.1	0.1-0.2	0.2-0.3	>0.3
crystal structure (ref. 32)	74	17	19	2	1
NR	64	20	21	3	1
S^2 _20	58	14	13	3	0
S^2 _200	50	23	13	2	0
NOE_20	42	0	0	0	0
NOE_1000	48	0	0	0	0
NOE_20_ S^2 _20	40	1	0	0	0
NOE_1000_ S^2 _20	47	0	0	0	0
NOE_IR	42	1	0	0	0
NOEred_IR	28	0	0	0	0
NOEred_20	34	0	0	0	0
NOEred_1000	46	0	0	0	0
NOEred_20_ S^2 _200	44	0	0	0	0
NOEred_1000_ S^2 _200	41	0	0	0	0

^{a)}For the analysis of the crystal structure and simulations NR to NOE_IR the original set of 1657 NOE bounds²⁰ was used, while for simulations NOEred_IR to NOEred_1000_ S^2 _200 the reduced set of 1646 NOE bounds was used. The 11 NOE bounds omitted are indicated in Figure 1. The 1657 NOE atom-atom pairs and bounds are specified in Table S1 of the Supporting Information.

Table 2: Number of deviations $|S_{\text{exp}}^2 - S_{\text{MD}}^2|$ of N-H bond vector S^2 order-parameter values derived from the various MD simulations and from experimental²¹ NMR data^{a)}.

Simulation	Size of S^2 deviation			
	0.05-0.1	0.1-0.2	0.2-0.3	>0.3
NR	29	16	6	2
S^2_{20}	35	10	3	0
S^2_{200}	17	1	0	0
NOE_20	26	23	14	7
NOE_1000	24	40	23	19
NOE_20_ S^2_{20}	44	23	4	1
NOE_1000_ S^2_{20}	31	37	12	4
NOE_IR	26	19	4	1
NOEred_IR	29	18	6	2
NOEred_20	24	22	9	6
NOEred_1000	21	34	12	7
NOEred_20_ S^2_{200}	19	2	0	0
NOEred_1000_ S^2_{200}	35	6	0	0

^{a)}The set of 113 S^2 order parameters is specified in Table S2 of the Supporting Information.

Table 3: Number of deviations $|^3J_{\text{exp}} - ^3J_{\text{MD}}|$ of backbone $^3J_{\text{H}_\text{N}\text{H}_\alpha}$ -coupling values derived from the various MD simulations and from experimental²⁰ NMR data^{a)}.

Simulation	Size of the $^3J_{\text{H}_\text{N}\text{H}_\alpha}$ deviation (in Hz)			
	0.5-1	1-2	2-3	>3
crystal structure (ref. 32)	12	20	7	4
NR	10	18	5	1
S^2 _20	13	16	2	1
S^2 _200	11	17	3	2
NOE_20	17	17	4	0
NOE_1000	22	14	4	0
NOE_20_ S^2 _20	19	11	3	1
NOE_1000_ S^2 _20	23	12	4	0
NOE_IR	16	15	3	1
NOEred_IR	18	14	3	1
NOEred_20	14	15	2	1
NOEred_1000	12	17	4	0
NOEred_20_ S^2 _200	10	18	1	2
NOEred_1000_ S^2 _200	19	12	5	0

^{a)}The set of 66 $^3J_{\text{H}_\text{N}\text{H}_\alpha}$ -couplings is specified in Table S3 of the Supporting Information.

Table 4: Average potential energy values in kJ mol^{-1} from the various 20 ns MD simulations^{a)}.

Simulation	distance restraints	S^2 restraints	protein	
			bonded terms	non-bonded terms
NR	0	0	4347	-15019
S^2 _20	0	5.7 (0.050)	4326	-14766
S^2 _200	0	4.8 (0.043)	4314	-14771
NOE_20	110 (0.067)	0	4480	-14449
NOE_1000	58 (0.035)	0	4529	-14240
NOE_20_ S^2 _20	118 (0.071)	6.0 (0.054)	4465	-14311
NOE_1000_ S^2 _20	52 (0.031)	5.9 (0.052)	4447	-14594
NOE_IR	231 (0.14)	0	4419	-14558
NOEred_IR	136 (0.08)	0	4326	-14626
NOEred_20	64 (0.038)	0	4405	-14540
NOEred_1000	33 (0.020)	0	4418	-14756
NOEred_20_ S^2 _200	71 (0.043)	7.3 (0.064)	4360	-14544
NOEred_1000_ S^2 _200	47 (0.028)	9.8 (0.086)	4406	-14362

^{a)}The values between parentheses are the restraint energies per NOE or S^2 restraint. For simulations NOE_20 to NOE_IR the original set of 1657 NOE bounds²⁰ was used, while for simulations NOEred_IR to NOEred_1000_ S^2 _200 the reduced set of 1646 NOE bounds was used. The 11 NOE bounds omitted are indicated in Figure 1. The protein energies are for the GROMOS 54A7 force field used.⁴¹

Table 5: Populations (%) of backbone hydrogen bonds in the AB2 and CD loops of IL-4 in the various 20 ns MD simulations^{a)}.

donor – acceptor	secondary structure	crystal structure	Simulation							
NH-CO			NR	S ² _20	S ² _200	NOE_20	NOE_20_S ² _20	NOERed_20	NOERed_20_S ² _200	
31-105	β	100	97	96	92	93	95	85	91	
36-103	β	0	63	0	0	0	0	0	1	
34-31	β_{10}	100	0	0	0	0	0	0	0	
35-31	α	0	0	18	0	19	11	68	46	
35-32	β_{10}	0	4	6	6	25	19	1	4	
36-32	α	0	0	4	1	0	11	7	17	
36-33	β_{10}	0	0	11	9	0	11	1	9	
37-33	α	0	0	0	1	0	1	3	2	
37-34	β_{10}	0	0	0	0	8	13	1	5	
38-34	α	0	0	0	0	12	3	0	0	
38-35	β_{10}	0	0	0	0	29	28	0	1	
39-35	α	0	0	0	0	11	14	0	0	
39-36	β_{10}	0	0	0	29	4	14	35	20	
65-61	α	0	0	0	0	0	0	0	0	
65-62	β_{10}	100	5	1	1	24	37	14	7	
66-62	α	100	93	97	97	50	38	57	38	
66-63	β_{10}	0	0	0	0	13	23	6	4	
67-63	α	0	52	41	51	35	23	26	1	
67-64	β_{10}	0	13	33	23	13	11	13	8	

^{a)} A hydrogen bond is present when the distance H-O is smaller than 0.25 nm and the angle N-H-O is larger than 135 degrees.

Acknowledgement

The authors gratefully acknowledge the contribution of Anoushka Mehta who, as a student at the University of Oxford, performed some preliminary work on IL-4 during the academic year 2013-2014. LJS would like to acknowledge the use of the University of Oxford Advanced Research Computing (ARC) facility in carrying out some of this work. <http://dx.doi.org/10.5281/zenodo.22558>. WFvG thanks the Swiss National Science Foundation, grant number 200020-137827, and the European Research Council, grant number 228076, for financial support. NH thanks the German Research Foundation (DFG) for financial support within the Cluster of Excellence in Simulation Technology (EXC 310/2) at the University of Stuttgart.

Supporting Information Available

Tables listing the experimental 1657 NOE distance bounds, 113 S^2 order parameter target values, and 66 $^3J_{\text{H}_\text{N}\text{H}_\alpha}$ -couplings for IL-4 together with values calculated from the simulation without any restraining (NR) and the simulation NOEred_20_ S^2 _200 with NOE distance and S^2 order parameter restraining.

This material is available free of charge via the Internet at <http://pubs.acs.org/>.

References

- (1) Kendrew, J. C.; Bodo, G.; Dintzis, H. M.; Parrish, R. G.; Wyckoff, H.; Phillips, D. C. A Three-Dimensional Model of the Myoglobin Molecule Obtained by X-Ray Analysis. *Nature* **1958**, *181*, 662–666.
- (2) Blake, C. C. F.; Koenig, D. F.; Mair, G. A.; North, A. C. T.; Phillips, D. C.; Sarma, V. R. Structure of Hen Egg-White Lysozyme: A Three-Dimensional Fourier Synthesis at 2 Å Resolution. *Nature* **1965**, *206*, 757–761.
- (3) Ernst, R. R.; Bodenhausen, G.; Wokaun, A. *Principles of Nuclear Magnetic Resonance in One and Two Dimensions*; Clarendon Press: Oxford, 1987.

- (4) Berndt, K. D.; Güntert, P.; Orbons, L. P.; Wüthrich, K. Determination of a High-Quality Nuclear Magnetic Resonance Solution Structure of the Bovine Pancreatic Trypsin Inhibitor and Comparison with Three Crystal Structures. *J. Mol. Biol.* **1992**, *227*, 757–775.
- (5) Berman, H. M.; Westbrook, J.; Feng, Z.; Gilliland, G.; Bhat, T. N.; Weissig, H.; Shindyalov, I. N.; Bourne, P. E. The Protein Data Bank. *Nucleic Acids Res.* **2000**, *28*, 235–242.
- (6) Tjandra, N.; Bax, A. Direct Measurement of Distances and Angles in Biomolecular NMR in a Dilute Liquid Crystalline Medium. *Science* **1997**, *278*, 1111–1114.
- (7) Wishart, D. S. Interpreting Protein Chemical Shift Data. *Prog. Nucl. Magn. Reson. Spectrosc.* **2011**, *58*, 62–87.
- (8) Karplus, M. Contact Electron-Spin Coupling of Nuclear Magnetic Moments. *J. Chem. Phys.* **1959**, *30*, 11–15.
- (9) Lipari, G.; Szabo, A. Model-free Approach to the Interpretation of Nuclear Magnetic Resonance Relaxation in Macromolecules. 1. Theory and Range of Validity. *J. Am. Chem. Soc.* **1982**, *104*, 4546–4559.
- (10) Henry, E. R.; Szabo, A. Influence of Vibrational Motion on Solid State Line Shapes and NMR Relaxation. *J. Chem. Phys.* **1985**, *82*, 4753–4761.
- (11) Hansen, N.; Heller, F.; Schmid, N.; van Gunsteren, W. F. Time-Averaged Order Parameter Restraints in Molecular Dynamics Simulations. *J. Biomol. NMR* **2014**, *60*, 169–187.
- (12) Smith, L. J.; van Gunsteren, W. F.; Hansen, N. Characterisation of the Flexible Lip Regions in Bacteriophage Lambda Lysozyme using MD Simulations. *Eur. Biophys. J.* **2015**, *44*, 235–247.

- (13) Smith, L. J.; Athill, R.; van Gunsteren, W. F.; Hansen, N. Interpretation of Seemingly Contradictory Data: Low NMR S^2 Order Parameters Observed in Helices and High NMR S^2 Order Parameters in Disordered Loops of the Protein hGH at Low pH. *Chem. Eur. J.* **2017**, DOI: 10.1002/chem.201700896.
- (14) Brünger, A. T. *X-PLOR, Version 3.1: A System for X-ray Crystallography and NMR*; Yale University Press: New Haven, CT, USA, 1992.
- (15) Kaptein, R.; Zuiderweg, E. R. P.; Scheek, R. M.; Boelens, R.; van Gunsteren, W. F. A Protein Structure from Nuclear Magnetic Resonance Data: Lac Repressor Headpiece. *J. Mol. Biol.* **1985**, *182*, 179–182.
- (16) Torda, A. E.; Scheek, R. M.; van Gunsteren, W. F. Time-Averaged Nuclear Overhauser Effect Distance Restraints Applied to Tendamistat. *J. Mol. Biol.* **1990**, *214*, 223–235.
- (17) Brünger, A. T.; Kuriyan, J.; Karplus, M. Crystallographic R Factor Refinement by Molecular Dynamics. *Science* **1987**, *235*, 458–460.
- (18) Gros, P.; van Gunsteren, W. F.; Hol, W. G. Inclusion of Thermal Motion in Crystallographic Structures by Restrained Molecular Dynamics. *Science* **1990**, *249*, 1149–1152.
- (19) van Gunsteren, W. F.; Allison, J. R.; Daura, X.; Dolenc, J.; Hansen, N.; Mark, A. E.; Oostenbrink, C.; Rusu, V. H.; Smith, L. J. Deriving Structural Information from Measured Data on Biomolecules. *Angew. Chem. Int. Ed.* **2016**, *55*, 15990–16010, *Angew. Chem.* **2016**, *128*, 16222–16244.
- (20) Smith, L. J.; Redfield, C.; Boyd, J.; Lawrence, G. M. P.; Edwards, R. G.; Smith, R. A. G.; Dobson, C. M. Human Interleukin 4: The Solution Structure of a Four-Helix Bundle Protein. *J. Mol. Biol.* **1992**, *224*, 899–904.
- (21) Redfield, C.; Boyd, J.; Smith, L. J.; Smith, R. A. G.; Dobson, C. M. Loop Mobility in

- a Four-Helix-Bundle Protein: Nitrogen-15 NMR Relaxation Measurements on Human Interleukin-4. *Biochemistry* **1992**, *31*, 10431–10437.
- (22) Paul, W. E. Interleukin-4: A Prototypic Immunoregulatory Lymphokine. *Blood* **1991**, *77*, 1859–1870.
- (23) Seder, R. A.; Paul, W. E. Acquisition of Lymphokine-Producing Phenotype by CD4⁺ T Cells. *Annu. Rev. Immunol.* **1994**, *12*, 635–673.
- (24) Nelms, K.; Keegan, A. D.; Zamorano, J.; Ryan, J. J.; Paul, W. E. The IL-4 Receptor: Signaling Mechanisms and Biologic Functions. *Annu. Rev. Immunol.* **1999**, *17*, 701–738.
- (25) Reinemer, P.; Sebald, W.; Duschl, A. The Interleukin-4-Receptor: From Recognition Mechanism to Pharmacological Target Structure. *Angew. Chem. Int. Ed.* **2000**, *39*, 2834–2846, *Angew. Chem.* **2000**, *112*, 2954–2966.
- (26) Powers, R.; Garrett, D. S.; March, C. J.; Frieden, E. A.; Gronenborn, A. M.; Clore, G. M. Three-Dimensional Solution Structure of Human Interleukin-4 by Multidimensional Heteronuclear Magnetic Resonance Spectroscopy. *Science* **1992**, *256*, 1673–1677.
- (27) Wlodawer, A.; Pavlovsky, A.; Gustchina, A. Crystal Structure of Human Recombinant Interleukin-4 at 2.25 Å Resolution. *FEBS Letters* **1992**, *309*, 59–64.
- (28) Walter, M. R.; Cook, W. J.; Zhao, B. G.; Cameron, R. P.; Ealick, S. E.; Walter, R. L.; Reichert, P.; Nagabhushan, T. L.; Trotta, P. P.; Bugg, C. E. Crystal Structure of Recombinant Human Interleukin-4. *J. Biol. Chem.* **1992**, *267*, 20371–20376.
- (29) Müller, T.; Oehlenschläger, F.; Buehner, M. Human Interleukin-4 and Variant R88Q: Phasing X-ray Diffraction Data by Molecular Replacement Using X-ray and Nuclear Magnetic Resonance Models. *J. Mol. Biol.* **1995**, *247*, 360–372.

- (30) Bazan, J. F. Structural Design and Molecular Evolution of a Cytokine Receptor Superfamily. *Proc. Natl. Acad. Sci. USA* **1990**, *87*, 6934–6938.
- (31) Smith, L. J.; Redfield, C.; Smith, R. A. G.; Dobson, C. M.; Clore, G. M.; Gronenborn, A. M.; Walter, M. R.; Naganbushan, T. L.; Wlodawer, A. Comparison of Four Independently Determined Structures of Human Recombinant Interleukin-4. *Nat. Struct. Biol.* **1994**, *1*, 301–310.
- (32) Kraich, M.; Klein, M.; Patiño, E.; Harrer, H.; Nickel, J.; Sebald, W.; Mueller, T. D. A Modular Interface of IL-4 Allows for Scalable Affinity Without Affecting Specificity for the IL-4 Receptor. *BMC Biology* **2006**, *4*, 13.
- (33) Redfield, C.; Smith, L. J.; Boyd, J.; Lawrence, G. M. P.; Edwards, R. G.; Gershater, C. J.; Smith, R. A. G.; Dobson, C. M. Analysis of the Solution Structure of Human Interleukin-4 Determined by Heteronuclear Three-Dimensional Nuclear Magnetic Resonance Techniques. *J. Mol. Biol.* **1994**, *238*, 23–41.
- (34) Dolenc, J.; Missimer, J. H.; Steinmetz, M. O.; van Gunsteren, W. F. Methods of NMR Structure Refinement: Molecular Dynamics Simulations Improve the Agreement with Measured NMR Data of a C-terminal Peptide of GCN4-p1. *J. Biomol. NMR* **2010**, *47*, 221–235.
- (35) Torda, A. E.; Scheek, R. M.; van Gunsteren, W. F. Time-Dependent Distance Restraints in Molecular Dynamics Simulations. *Chem. Phys. Lett.* **1989**, *157*, 289–294.
- (36) Winger, M.; Yu, H.; Redfield, C.; Van Gunsteren, W. F. Molecular Dynamics Simulation of Human Interleukin-4: Comparison with NMR Data and Effect of pH, Counterions and Force Field on Tertiary Structure Stability. *Molec. Simul.* **2007**, *33*, 1143–1154.
- (37) Schuler, L. D.; Daura, X.; van Gunsteren, W. F. An Improved GROMOS96 Force Field for Aliphatic Hydrocarbons in the Condensed Phase. *J. Comput. Chem.* **2001**, *22*, 1205–1218.

- (38) Oostenbrink, C.; Villa, A.; Mark, A. E.; Van Gunsteren, W. F. A Biomolecular Force Field Based on the Free Enthalpy of Hydration and Solvation: The GROMOS Force-Field Parameter Sets 53A5 and 53A6. *J. Comput. Chem.* **2004**, *25*, 1656–1676.
- (39) van Gunsteren et al., W. F. GROMOS. <http://www.gromos.net/>.
- (40) Schmid, N.; Allison, J. R.; Dolenc, J.; Eichenberger, A. P.; Kunz, A.-P. E.; van Gunsteren, W. F. Biomolecular Structure Refinement Using the GROMOS Simulation Software. *J. Biomol. NMR* **2011**, *51*, 265–281.
- (41) Schmid, N.; Eichenberger, A. P.; Choutko, A.; Riniker, S.; Winger, M.; Mark, A. E.; van Gunsteren, W. F. Definition and Testing of the GROMOS Force-Field Versions 54A7 and 54B7. *Eur. Biophys. J.* **2011**, *40*, 843–856.
- (42) Berendsen, H. J. C.; Postma, J. P. M.; van Gunsteren, W. F.; Hermans, J. In *Intermolecular Forces*; Pullmann, B., Ed.; Reidel: Dordrecht, the Netherlands, 1981; pp 331–342.
- (43) Ryckaert, J. P.; Ciccotti, G.; Berendsen, H. J. C. Numerical Integration of the Cartesian Equations of Motion of a System With Constraints: Molecular Dynamics of *n*-Alkanes. *J. Comput. Phys* **1977**, 327–341.
- (44) Hockney, R. W.; Eastwood, J. W. *Computer Simulation Using Particles*; McGraw-Hill: New York, 1981.
- (45) van Gunsteren, W. F.; Berendsen, H. J. C.; Geurtsen, R. G.; Zwinderman, H. R. J. A Molecular Dynamics Computer Simulation of an Eight-Base-Pair DNA Fragment in Aqueous Solution: Comparison with Experimental Two-Dimensional NMR Data. *Ann. N. Y. Acad. Sci.* **1986**, *482*, 287–303.
- (46) Barker, J. A.; Watts, R. O. Monte Carlo Studies of the Dielectric Properties of Water-Like Models. *Mol. Phys.* **1973**, *26*, 789–792.

- (47) Tironi, I. G.; Sperb, R.; Smith, P. E.; van Gunsteren, W. F. A Generalized Reaction Field Method for Molecular Dynamics Simulations. *J. Chem. Phys.* **1995**, *102*, 5451–5459.
- (48) Heinz, T. N.; van Gunsteren, W. F.; Hünenberger, P. H. Comparison of Four Methods to Compute the Dielectric Permittivity of Liquids from Molecular Dynamics Simulations. *J. Chem. Phys.* **2001**, *115*, 1125–1136.
- (49) van Gunsteren, W. F.; Boelens, R.; Kaptein, R.; Scheek, R. M.; Zuiderweg, E. R. P. In *Molecular Dynamics and Protein Structure*; Hermans, J., Ed.; Polycrystal Book Service: Western Springs, 1985; pp 92–99.
- (50) Wüthrich, K.; Billeter, M.; Braun, W. Pseudo-Structures for the 20 Common Amino Acids for use in Studies of Protein Conformations by Measurements of Intramolecular Proton-Proton Distance Constraints with Nuclear Magnetic Resonance. *J. Mol. Biol.* **1983**, *169*, 949–961.
- (51) Yip, P.; Case, D. A. A New Method for Refinement of Macromolecular Structures Based on Nuclear Overhauser Effect Spectra. *J. Magn. Reson.* **1989**, *83*, 643–648.
- (52) Peter, C.; Daura, X.; van Gunsteren, W. F. Calculation of NMR-Relaxation Parameters for Flexible Molecules from Molecular Dynamics Simulations. *J. Biomol. NMR* **2001**, *20*, 297–310.
- (53) Schmid, N.; Allison, J. R.; Dolenc, J.; Eichenberger, A. P.; Kunz, A.-P. E.; van Gunsteren, W. F. Biomolecular Structure Refinement Using the GROMOS Simulation Software. *J. Biomol. NMR* **2011**, *51*, 265–281.
- (54) Chalmers, G.; Glushka, J. N.; Foley, B. L.; Woods, R. J.; Prestegard, J. H. Direct NOE Simulation from Long MD Trajectories. *J. Magn. Reson.* **2016**, *265*, 1–9.

TOC Graphic

